

# Novel Metal Clusters Isolated from Blood Are Lethal to Cancer Cells

Alexander M. Samoylov<sup>a</sup> Tatiana I. Samoylova<sup>b</sup> Oleg M. Pustovyy<sup>a</sup>  
Alexei A. Samoylov<sup>a</sup> Maria A. Toivio-Kinnucan<sup>c</sup> Nancy E. Morrison<sup>b</sup>  
Ludmila P. Globa<sup>b</sup> William F. Gale<sup>d</sup> Vitaly Vodyanoy<sup>a</sup>

<sup>a</sup>Department of Anatomy, Physiology and Pharmacology, <sup>b</sup>Scott-Ritchey Research Center, and  
<sup>c</sup>Department of Pathobiology, College of Veterinary Medicine, and <sup>d</sup>Materials Research and Education Center,  
Samuel Ginn College of Engineering, Auburn University, Auburn, Ala., USA

## Key Words

Aggregation · Nucleating centers · Blood · Metallic nanoclusters · Protein

## Abstract

Unfolding and subsequent aggregation of proteins is a common phenomenon that is linked to many human disorders. Misfolded hemoglobin is generally manifested in various autoimmune, infectious and inherited diseases. We isolated micrometer and submicrometer parti-

cles, termed proteons, from human and animal blood. Proteons lack nucleic acids but contain two major polypeptide populations with homology to the hemoglobin  $\alpha$ -chain. Proteons form by reversible seeded aggregation of proteins around proteon nucleating centers (PNCs). PNCs are comprised of 1- to 2-nm metallic nanoclusters containing 40–300 atoms. Each milliliter of human blood contained approximately  $7 \times 10^{13}$  PNCs and approximately  $3 \times 10^8$  proteons. Exposure of isolated blood plasma to elevated temperatures increased the number of proteons. When an aliquot of this heated plas-

## Abbreviations used in this paper

ATCC	American type culture collection	EDTA	ethylenediaminetetraacetate
Annexin V-FITC	Calbiochem Annexin V- FITC (fluorescein isothiocyanate) apoptosis detection kit	FCC	face-centered cubic
BF	bright field	FCS	fetal calf serum
BCC	body-centered cubic	Hb	hemoglobin
D5648	D5648 tissue culture medium (Sigma) with 10% FBS (HyClone) (culture medium 1)	LDF	dark-field light microscopy
D6429	D6429 tissue culture medium (Sigma) with 10% FBS (HyClone) (culture medium 2)	MTT	tetrazolium salt (3-[4,5-dimethylthiazol-2-yl]-2,5-diphenyl tetrazolium bromide); proteon-nucleating center
DF	dark field	PNC	proteon-nucleating center
DMEM	Dulbecco's modified Eagle's medium	PrP <sup>Sc</sup>	misfolded prion protein molecule
DMSO	dimethyl sulfoxide	SAD	selected area diffraction
EM	electron microscopy	SDS	sodium dodecyl sulfate
EDS	energy-dispersive X-ray spectroscopy	SEM	scanning electron microscopy
		TEM	transmission electron microscopy
		UTW	ultrathin window

ma was introduced into untreated plasma that was subsequently heated, the number of proteons further increased, reaching a maximum after a total of three such iterations. Small concentrations of PNCs were lethal to cultured cancer cells, whereas noncancerous cells were much less affected.

Copyright © 2005 S. Karger AG, Basel

## Introduction

Unfolding and subsequent aggregation of proteins is a common phenomenon linked to many human disorders [Carrel and Lomas, 1997]. Misfolded hemoglobin (Hb) is associated with intravascular hemolysis that manifests in various autoimmune, infectious and inherited diseases [Schluter and Drenckhahn, 1986; Kannan, et al., 1988; Deiss, 1999; Papalexis et al., 2001]. Hemolysis results in the release of Hb and fragments thereof, both of which are scavenged by the haptoglobin pathway [Deiss, 1999]. We investigated a possible mechanism by which excess Hb release may be controlled/regulated in blood plasma in the disease state. We found that human blood contains metallic-based particles called proteons that may reinforce haptoglobin-mediated Hb scavenging.

## Materials and Methods

### *Replication of Proteons from Blood*

Freshly drawn blood (30  $\mu$ l) from healthy male subjects (human, rabbit, or dog) was diluted to 1 ml with purified water (Direct QTM, Millipore, 17 M $\Omega$ ) in a 1.5-ml plastic tube and centrifuged at 13,000 g for 5 min at room temperature. The plasma supernatant was used to prepare both proteons and proteon nucleating centers (PNCs). To produce proteons, the supernatant was transferred to a 4-ml glass vial with a plastic cap with a Teflon liner and subjected to 120°C at 140 kPa for 2 h. The PNC suspension (filtrate) was obtained by filtering the plasma supernatant consecutively through 30- and 5-kDa Centricon filters (Millipore).

### *Protein Analyses*

Chemical composition was determined by energy-dispersive X-ray spectroscopy (EDS) using a JEOL JSM-840 scanning electron microscope with an Oxford Instruments ultrathin window (UTW) X-ray detector and an Oxford ISIS analyzer. The protein content of proteons was determined using Bio-Rad assays. Protein fragments from proteons were isolated by sodium dodecyl sulfate (SDS)-polyacrylamide gel electrophoresis, and identified by amino acid sequencing (University of Alabama Protein Analysis Laboratory).

### *Nucleic Acids*

DNA was isolated and purified using the DNeasy tissue kit (Qiagen). Nucleic acids were also isolated using the High Pure PCR tem-

plate preparation kit (Roche). DNA was detected in plasma but not in proteons. Fluorometric analysis of double-stranded DNA was accomplished with the PicoGreen dsDNA quantitation reagent (Molecular Probes) and the Tecan SPECTRAFluor Plus spectrometer using DeltaSOFT software (485 nm excitation, 535 nm emission).

### *Microscopy*

TEM was performed using a JEOL JEM 2010 instrument at 200 kV. Bright-field imaging (BF) provided an overview of the microstructure of the sample. Detailed structures were characterized by selected area diffraction (SAD) and nanobeam diffraction, the latter producing a narrow (<50-nm diameter) yet nearly parallel beam that produced SAD-like patterns. DF (dark field) was employed to determine which microstructural features gave rise to diffraction maxima. Care was taken to avoid excessive beam-induced sample heating. Microstructural feature composition was qualitatively determined by EDS using the JEM 2010, the UTW detector and the ISIS analyzer. SEM images were obtained using the JSM-840. PNCs were precipitated by gravity from the PNC suspension with 1.2 mM MgSO<sub>4</sub> (pH 11.3) at room temperature for 16 h. Aliquots of the precipitate (2  $\mu$ l) were transferred to 400-mesh Ni/carbon grids (Electron Microscopy Sciences) and dried overnight at room temperature. Proteon samples for transmission electron microscopy (TEM) were fixed with 3% glutaraldehyde, dehydrated with ethanol and embedded in Durcupan ASM resin (Fluka). Proteons and cells were visualized with an Olympus microscope fitted with a 100-watt mercury lamp, a polarizer, a Naessens DF condenser (Cose Corp.) and a 100 $\times$  objective (oil, NA 1.4). DF images were directed to a DEI-470T CCD video camera system (Optronics Engineering) and captured with a 1.0 Pro Series capture kit using 2.0 Image-Pro Plus software (Media Cybernetics), providing high-resolution direct-view optical images in real time. The samples were observed in an aqueous environment and required no freezing, dehydration, staining, shadowing, marking or any other manipulation.

### *Metals*

Metals in proteons and PNCs were identified by EDS and inductively coupled plasma-atomic emission spectrometry (GTW Analytical Services).

### *Cell Culture*

RG2, F98, Hs683 (rat and human brain glioma lines), CTX TNA2 (brain rat astrocytes transfected with SV40), H9c2[2-1] (rat heart myocardium), 27FR (rat skin fibroblast), and SVGp12 (human brain astroglia) cells were obtained from American Type Culture Collection (ATCC) and maintained as recommended by ATCC. A cell proliferation assay quantitatively determined the effect of proteons and PNCs on cell viability. Cells were plated in D5648 media (Sigma) containing 10% fetal calf serum (FCS; HyClone) in 96-well polystyrene plates at a density of  $3 \times 10^3$  cells/well. At 24 h after plating, the medium was replaced with Dulbecco's Modified Eagle's Medium (DMEM; 100  $\mu$ l/well) containing either 1  $\mu$ M staurosporine or  $1-1,000 \times 10^9$  PNCs/ml. PNCs were autoclaved at 120°C at 140 kPa for 15 min before addition. At 20 h after treatment, a 20- $\mu$ l aliquot of tetrazolium salt (3-[4,5-dimethylthiazol-2-yl]-2,5-diphenyl tetrazolium bromide; MTT, 5 mg/ml in PBS) was added to each well, and the cells were incubated for 4 h at 37°C. MTT was reduced in metabolically active cells to form purple formazan crystals that were subsequently dissolved in di-

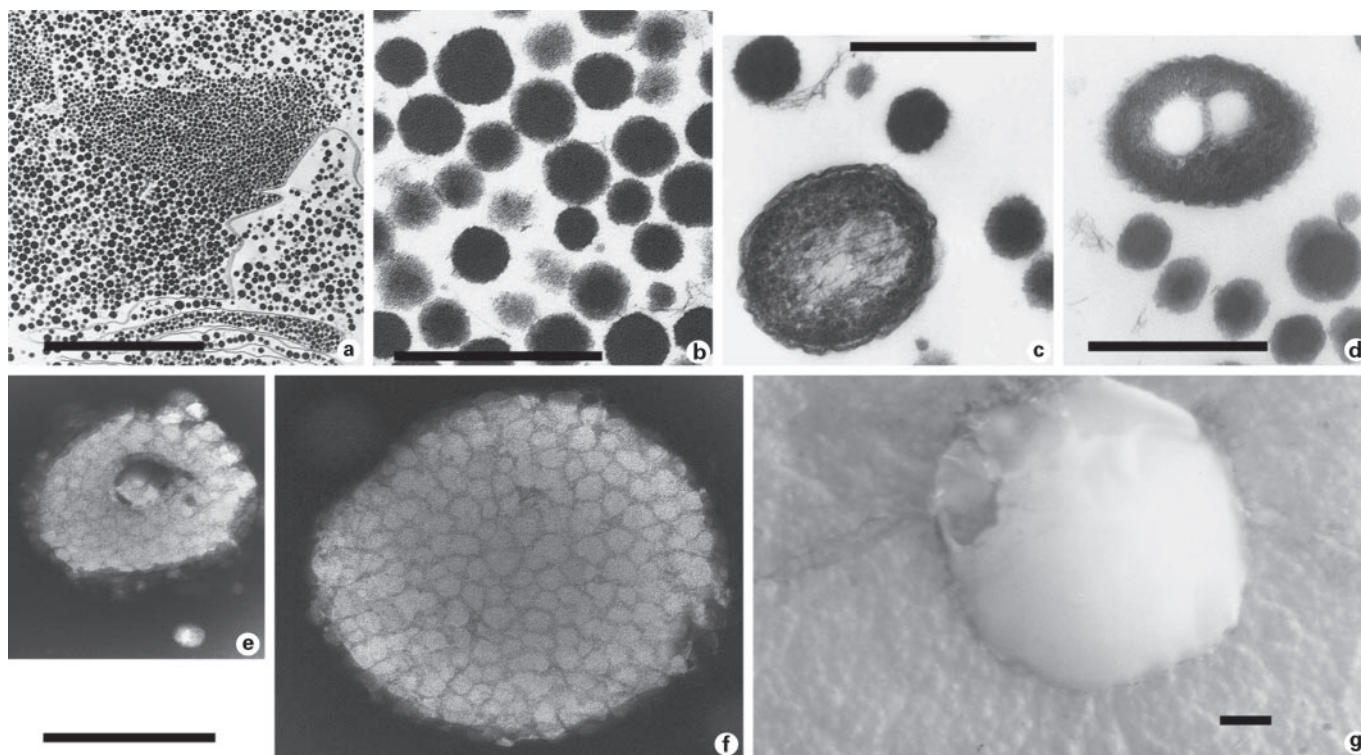


**Fig. 1.** Electron micrographs of proteons. TEM of thin sections of type 1 (**a, b**) and type 2 (**c, d**) proteons. **e, f** TEM of negatively stained type 2 proteons. **g** SEM of a type 2 proteon. Scale bars: **a** 5  $\mu\text{m}$ ; **b–f** 0.5  $\mu\text{m}$ ; **g** 1  $\mu\text{m}$ .

methyl sulfoxide (DMSO) and quantified by a plate reader (BioRad). Apoptosis was evaluated with ApoAlert (BD Biosciences). Cells were trypsinized, counted, and plated at  $1 \times 10^5$  cells/well onto 4-chamber tissue culture-treated slides (Nunc Lab-Tek II chamber slide, Fisher). After culturing for 24 h, cells were exposed to  $7.7 \times 10^{11}$  PNCs/ml from shark blood, then stained with Annexin V-FITC and propidium iodide. (Shark's blood contains approximately 5-fold more PNCs/ml than rat or rabbit blood.) Cells were then analyzed with a Nikon Eclipse E600 fluorescence microscope.

#### *Proteon Proliferation*

Two sets of samples were prepared, one of which was incubated at 37°C in ambient air whereas the other was incubated in 5% CO<sub>2</sub> in air. Duplicate samples in each set contained either 3 ml of a water suspension containing  $7.3 \times 10^{10}$  proteons/ml, 3 ml plasma, or 10  $\mu\text{l}$  of the same proteon suspension in 3 ml of D6429 (or D5648) tissue culture medium (Sigma) containing 10% FBS (HyClone). Uninoculated media served as negative controls. Samples were tested after 0, 2, 4, 8 and 13 days. After proteons were allowed to proliferate in the presence of 8 M urea, the proteon suspension was dialyzed (Pierce Slide-A-Lyser 10K, 20 h, 20°C) against 5 liters of purified water. Proteons were then counted and analyzed using DF light microscopy (LDF) and electron microscopy (EM).

## **Results**

### *Structure of Proteons*

Healthy human blood samples typically contained approximately  $3 \times 10^8$  proteons/ml, with a maximum of approximately  $3 \times 10^{11}$ . Proteons appeared as particles of 0.05–5  $\mu\text{m}$  in size when observed by TEM or scanning EM (SEM; fig. 1). Using LDF, proteons in liquid samples appeared as bright dots that moved rapidly and randomly. By TEM, small proteons (type 1) appeared as dark disks as shown in figure 1a (showing an approximately 100- $\mu\text{m}^2$  area) and figure 1b (an approximately 0.7- $\mu\text{m}^2$  area), the diameter of which ranged from 50 to 250 nm. TEM also revealed larger coconut-shaped proteons (type 2) that exhibited a long axis of 1–5  $\mu\text{m}$  and contained one or more nuclei (fig. 1c–g). Type 2 proteons exhibited a cell-like form (fig. 1c) with an external membrane-like structure, although their appearance was distinct from bacterial walls or the mammalian plasma membrane. Rather, this external structure appeared as a curly fibrous shell with a thickness of 10–12 nm. Fiber-like structures

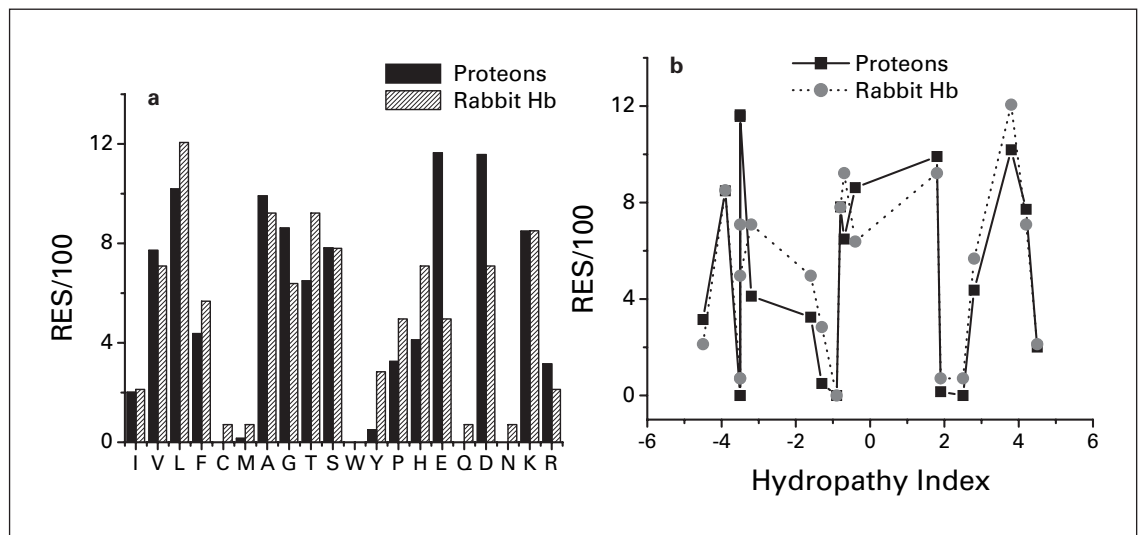


**Fig. 2.** Comparison of the amino acid composition of proteons and rabbit Hb. **a** Distribution of amino acids in proteons and rabbit Hb. The letters correspond to the International Union of Pure and Applied Chemistry single-letter amino acid code. **b** Number of amino acids as a function of the hydropathy index [Kyte and Doolittle, 1982]. The negatively charged residues glutamic acid and aspartic acid are highly represented relative to other residues.

and a few nuclei were visible inside some type 2 proteons (fig. 1c), whereas more distinct nuclei were visible inside others (fig. 1d). Multiple nuclei are shown in figure 1e, f, in which the type 2 proteon seems to be porous and actively expelling nuclei. These nuclei were very similar in appearance to the smaller type 1 proteons. The appearance of type 2 proteons was comparable in images from TEM (fig. 1e, f) and SEM (fig. 1g). Figure 1g shows a large type 2 proteon with a sizeable pore positioned on a bed of smaller type 1 proteons. Additionally, fibrous or filamentous structures of varying morphology were observed regardless of the microscopic technique. Some fibrous structures were shapeless bundles that filled the space between proteons, whereas others were positioned either in the outer shells or inside larger proteons (fig. 1c). In many samples, large areas were covered with this fiber-like matter in coexistence with an abundance of type 1 proteons. Given that similar images were obtained with two different EM techniques and by LDF (in which samples were not subjected to physical or chemical treatment), it is highly unlikely that the proteons we observed were artifacts of sample preparation. Furthermore, proteons were also observed in untreated blood plasma. Finally, proteons were not the result of biological contamination because the samples were prepared and maintained under sterile conditions.

#### *Chemical Composition of Proteons*

EDS revealed that proteons from human blood are composed primarily of carbon, oxygen, nitrogen and sulfur (data not shown; lighter elements such as hydrogen cannot be detected by this technique). Minute levels of potassium, sodium, chlorine, zinc and copper were also detected. Quantitative assays (Bio-Rad protein assay, Qiagen Dneasy kit, and Roche High Pure PCR kit) demonstrated that proteons contain proteins but no nucleic acids (data not shown). Rabbit blood proteons were disassembled using the negatively charged detergent SDS, and subsequent denaturing polyacrylamide gel electrophoresis revealed distinct protein bands of 14.4 and 8 kDa (data not shown). N-terminal amino acid sequencing of both fragments yielded the partial sequence VLSPA(D/E)(E/K)TN(A/I), which is 100% identical to a sequence within the rabbit Hb  $\alpha$ -chain [Vonehren, 1966]. Amino acid analysis showed that, relative to rabbit Hb, proteons are enriched in the negatively charged residues glutamic acid and aspartic acid (fig. 2). Staining of proteons with Congo red resulted in apple-green birefringence under polarized light [Kelly, 1996], indicating the anisotropic alignment of dye molecules (fig. 3), which is similar to that observed with prions [Korth et al., 1997].

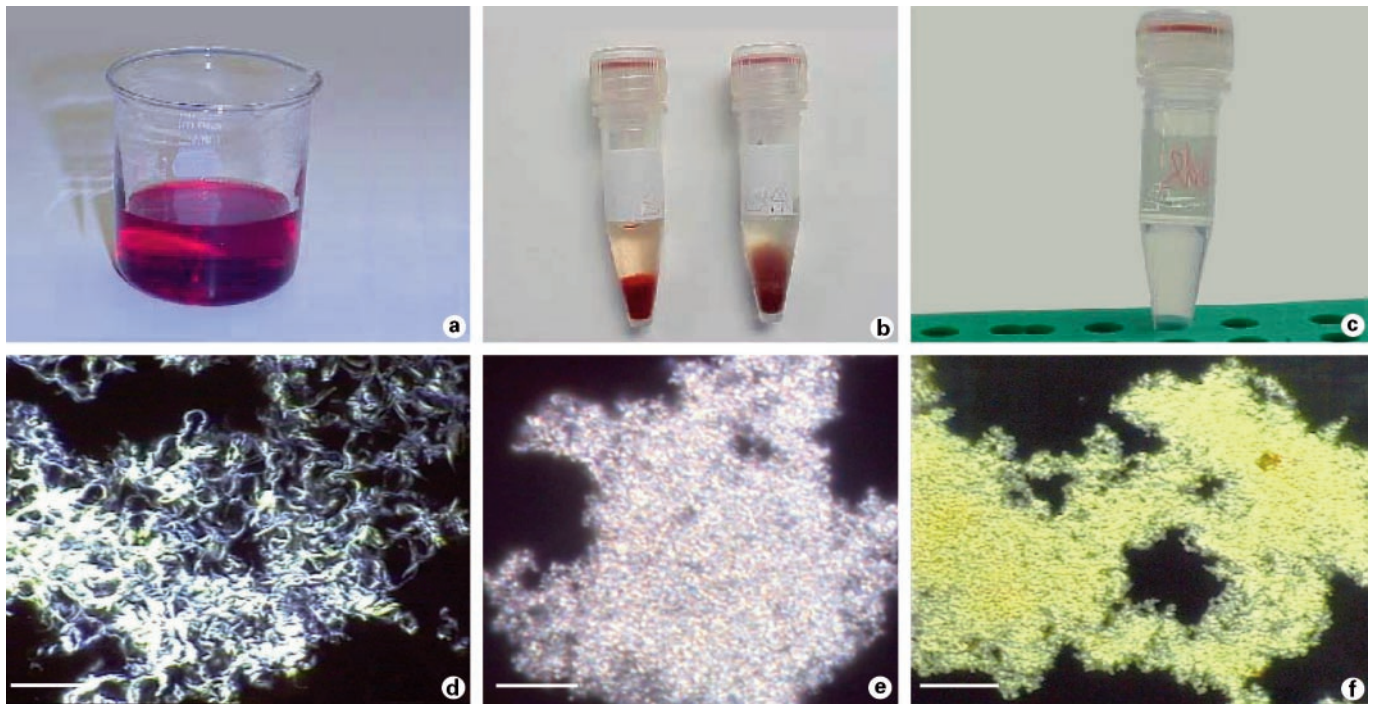


**Fig. 3.** Interaction of Congo red with proteons. **a** Water solution of Congo red dye in a glass beaker. **b** A suspension of proteons obtained from rabbit blood (right), and rabbit proteons stained with Congo red (left). **c** Water suspension of PNCs. **d** DF micrograph of precipitated PNCs treated with Congo red. **e** DF micrograph of precipitated proteons. **f** DF micrograph of precipitated proteons treated with Congo red. Staining of proteons with congo-red resulted in apple-green birefringence under polarized light [Kelly, 1996], indicating the anisotropic alignment of dye molecules similar to that observed with prions [Korth et al., 1997]. Scale bars: 10  $\mu\text{m}$ .

### Proteon Proliferation

When proteons were incubated at 37°C in purified water in ambient air, the number of particles did not change over 13 days ( $p < 0.01$ ) as determined by LDF (fig. 4a). Under the same conditions, the number of proteons in a plasma sample remained essentially constant over the first 8 days, but increased dramatically thereafter, equaling the number of proteons in the water sample after 13 days (fig. 4a). Proteons and plasma incubated in culture medium yielded essentially identical proliferation curves, reaching the same number of proteons after 13 days (fig. 4b;  $t_{1/2} = 8$  days). The culture medium alone contained no proteons and served as a negative control (fig. 4b). The  $\text{CO}_2$  level did not influence proteon proliferation ( $p < 0.01$ ; data not shown).

To test the hypothesis that proteons proliferate primarily via nucleation and growth, we exposed plasma samples to elevated temperature (120°C) and pressure (~140 kPa) in combination with increasing concentrations of the chaotropic agents urea and guanidinium hydrochloride, which denature proteins and prevent aggre-

gation [Logan et al., 1994]. The number of proteons decreased with increasing urea (fig. 4c; similar results were obtained with guanidinium hydrochloride). When a plasma sample that was treated with 8 M urea was subsequently dialyzed, the number of proteons increased significantly (fig. 4c, star). These experiments are consistent with a process by which proteons form from preexisting PNCs that serve as nuclei for misfolded protein aggregation, and thereby provide a methodology for the assembly and disassembly of proteons in vitro.

As demonstrated above, the visible number of proteons in plasma increased with elevated temperature and pressure. This amplification became more efficient, however, when we added a small portion of a previously heated sample to untreated plasma that was subsequently heated. Additional rounds of this procedure yielded a substantial increase in the proteon population. After a slight but significant increase in proteons during the first two cycles, the third cycle resulted in a dramatic increase that represented the saturation point of the system

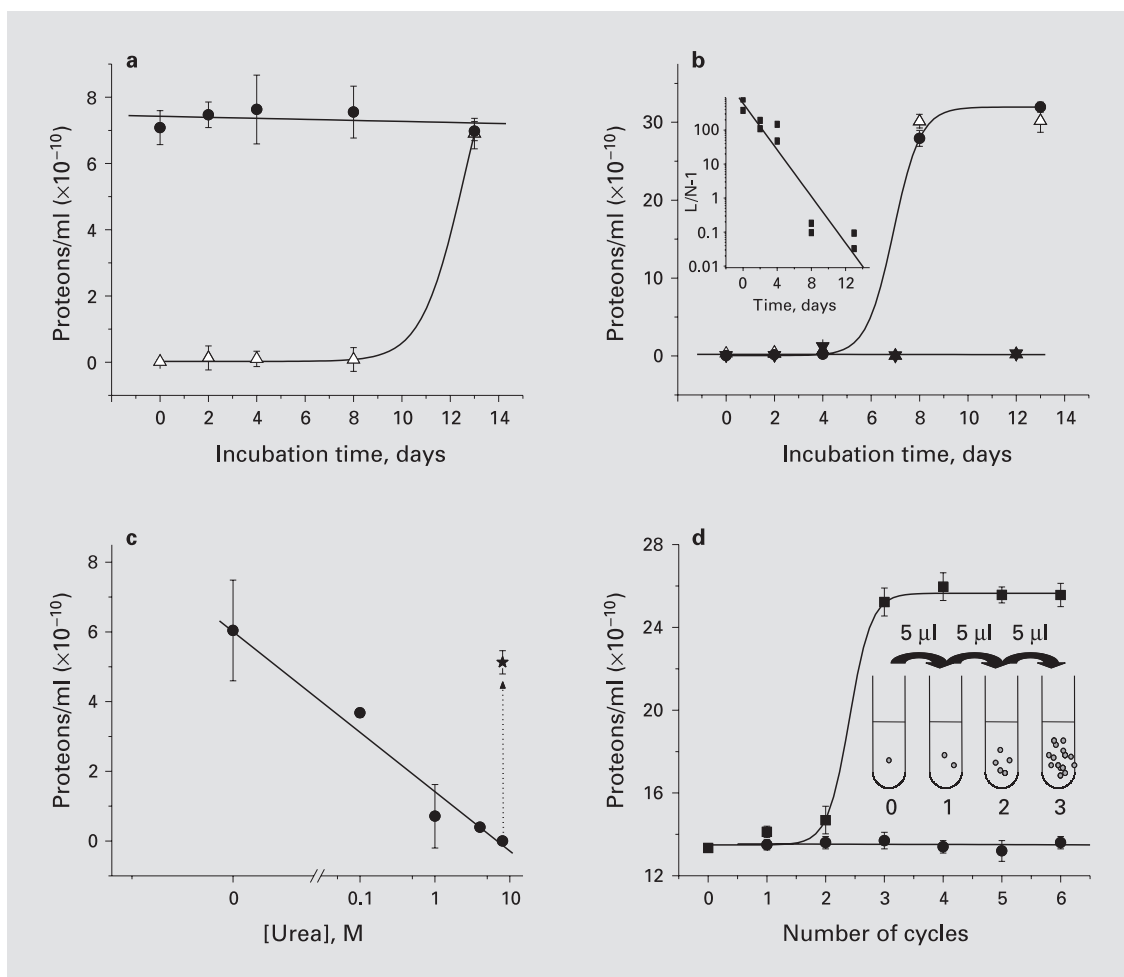


**Fig. 4.** Proliferation of proteons. **a** The number of proteons as a function of time, visualized by LDF. Proteons in purified water (●) or in blood plasma ( $\Delta$ ) were incubated at 37°C in ambient air. **b** Proteons (●) and plasma ( $\Delta$ ) incubated in tissue culture medium. D5648 ( $\blacktriangle$ ) and D6429 ( $\blacktriangledown$ ) media served as negative controls. The insert shows a linear fit of the experimental data to the equation [Jarman, 1970]  $\ln(L/N - 1) = k(T_{1/2} - t)$ , where  $L$  is the maximum number of proteons,  $N$  is number of proteons at time  $t$ , and  $T_{1/2}$  is the time at which  $N = L/2$ . **c** Assembly and disassembly of proteons

in the absence or presence of urea. After proteon assembly in the presence of varying concentrations of urea (●), the urea was removed from the proteon suspensions by dialysis (dotted arrow, ★). **d** Cyclic amplification of proteons in plasma. The first sample was incubated for 15 min at 65°C under ambient pressure. Five microliters of this sample was then added to 1 ml of the untreated second sample that was then treated as above. This process was repeated for a total of six cycles (■). A control series was run by adding of 5  $\mu$ l of water (instead of sample) to 1 ml of untreated plasma (●).

(fig. 4d). This cyclic amplification procedure can be utilized to detect low levels of proteons in samples, in a manner similar to that used to detect small quantities of misfolded prion proteins via cycles of ultrasound-induced amplification [Saborio et al., 2001].

#### Proteon Nucleating Centers

When PNCs were removed from blood plasma by filtration through a 5-kDa filter, the amount of protein in

the retentate was equivalent to that of the nonfiltered sample, and no protein was found in the filtrate (data not shown). Proteons could not be produced from the retentate until an aliquot of the filtrate was added back, and proteon production was dependent on the amount of filtrate added (data not shown). Interestingly, proteons could be produced in this manner even after the filtrate was carbonized at 660°C, but production was quenched by 10 mM EDTA, a metal-chelating agent (data not

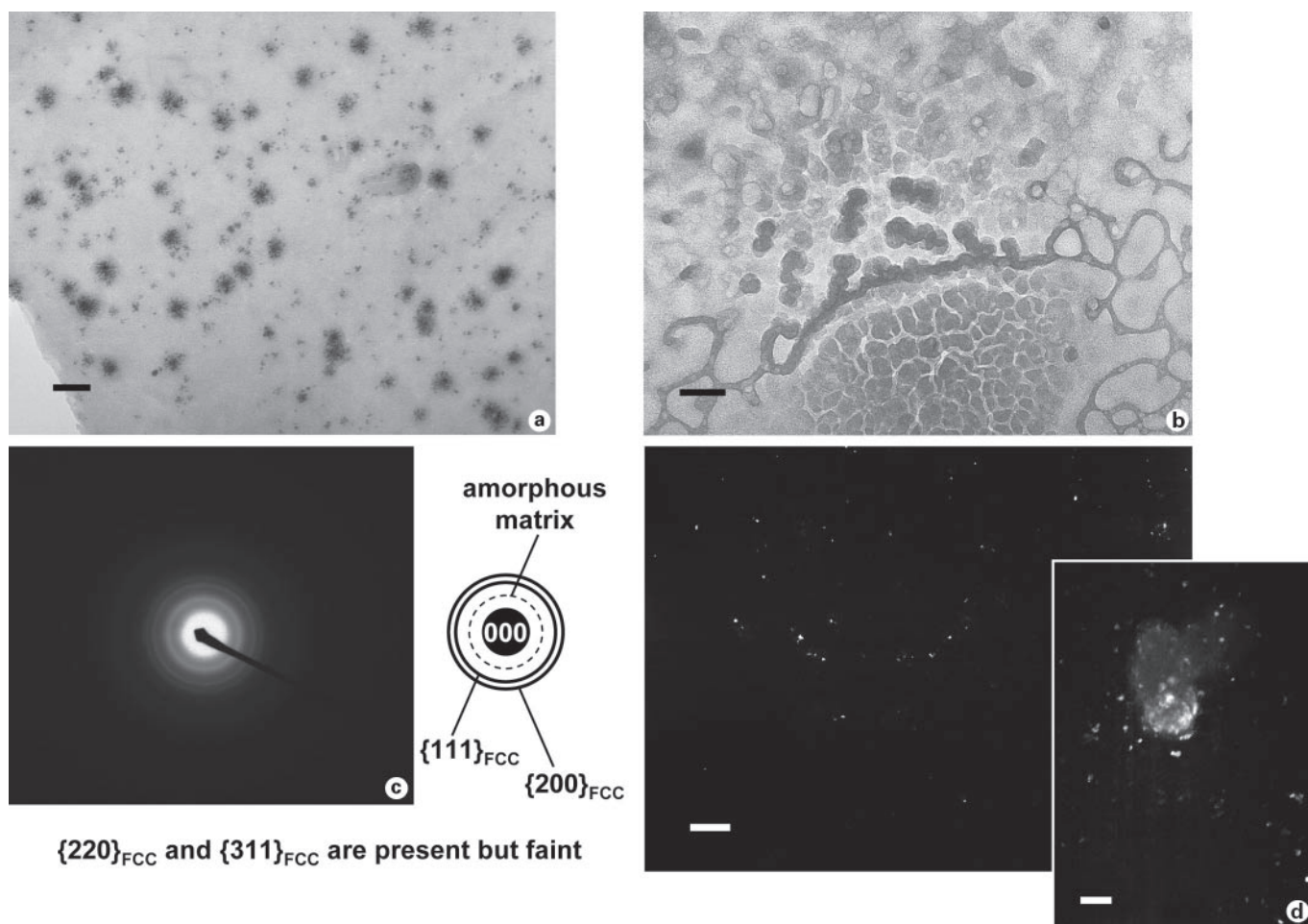


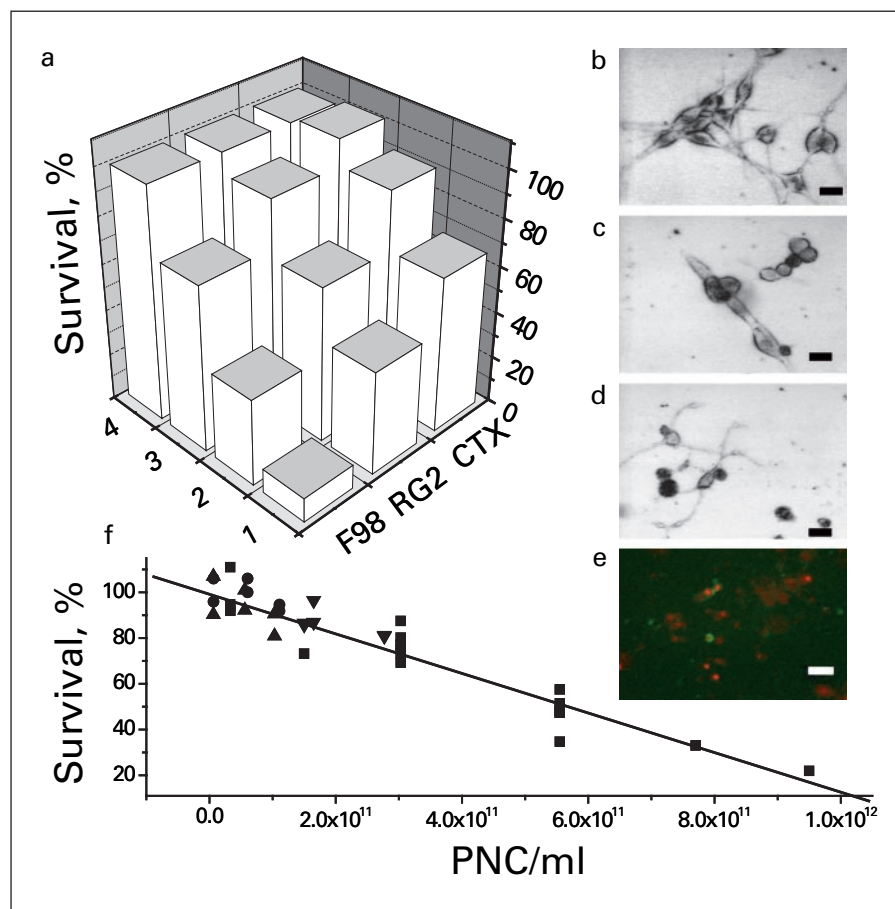
**Fig. 5.** Characterization of the Cu metal-containing nanoparticles using TEM, with  $\alpha$ -Fe-containing particles shown for comparison. **a** BF image showing clusters of crystalline metallic Cu nanoparticles. **b** BF image of the amorphous matrix, for comparison with **(a)**. **c** SAD pattern identifying the nanoparticles in **a** as an FCC phase with a lattice parameter of  $\sim 360$  pm and random crystallographic orientation. **d** Centered DF image prepared using a portion of the  $\{111\}_{\text{FCC}}$  ring, as shown in **c**. The nanoparticles appear bright on a dark background, indicating that the  $\{111\}_{\text{FCC}}$  diffraction maxima originated from the nanoparticles and not the matrix (since the Cu particles are randomly oriented, many of the particles are out of contrast). The inset shows clumped and individual  $\alpha$ -Fe particles (DF from a portion of the  $\{110\}_{\text{BCC}}$  ring). Scale bars: **a**, **b**, **d** 50 nm; insert 20 nm.

shown) [Irving and Al-Jarrah, 1975]. Adsorption spectra (GTW Analytical Services) of the filtrate revealed the presence of metals, namely Cu, Zn and Fe (data not shown).

TEM showed that the bulk of the dried PNC-containing filtrate was amorphous, and that it contained crystalline metallic nanoparticles of 1–2 nm in diameter (fig. 5a, d). SAD patterns from different regions of the samples were consistent with both face-centered cubic (FCC) and body-centered cubic (BCC) metals, with lattice parameters ( $a_0$ ) of  $\sim 360$  and  $\sim 290$  pm, respectively (fig. 5c). FCC

and BCC lattices belong to the family of Bravais lattices, which are distinct lattice types that, when repeated, can fill the entire space. These lattice features and  $a_0$  data are consistent with FCC copper ( $a_0 = 361.50$  pm) and BCC  $\alpha$ -iron ('ferrite';  $a_0 = 286.64$  pm) [Powder, 2001]. Furthermore, both copper and iron were identified from EDS spectra acquired from regions containing the nanoparticles (data not shown), and centered DF indicated that the diffraction maxima originated from the nanoparticles. Importantly, the observed crystallography of nonclumped nanoparticles was that of metallic iron and copper rather

**Fig. 6.** Effect of PNCs on cell viability. **a** Viability of cultured cells after a 20-hour exposure to different concentrations of PNCs (obtained from shark blood). Row 1:  $1.7 \times 10^{11}$  PNCs/ml; row 2:  $9.1 \times 10^{10}$ ; row 3:  $9.9 \times 10^9$ ; row 4: no PNCs. F98 and RG2 represent rat brain glioma cells and CTX represents rat astrocytes. **b–d** LDF images of rat glioma cells. **b, c** Cells before and after exposure to  $7.7 \times 10^{11}$  PNCs/ml, respectively. **d** Cells after exposure to  $1.0 \mu\text{M}$  staurosporine. **e** Fluorescence photomicrograph of RG2 glioma cells exposed to  $7.7 \times 10^{11}$  PNCs/ml for 30 min and stained with annexin V and propidium iodide. **f** Viability of cultured RG2 after a 20-hour exposure to different concentrations of PNCs obtained from the blood of the blue shark (*Prionace*; ■), dog (●), human (▲), or New Zealand white rabbit (Harland Sprague-Dawley) (▼).  $R^2 = 0.95$ ;  $p < 0.0001$ . Scale bars: 40  $\mu\text{m}$ .

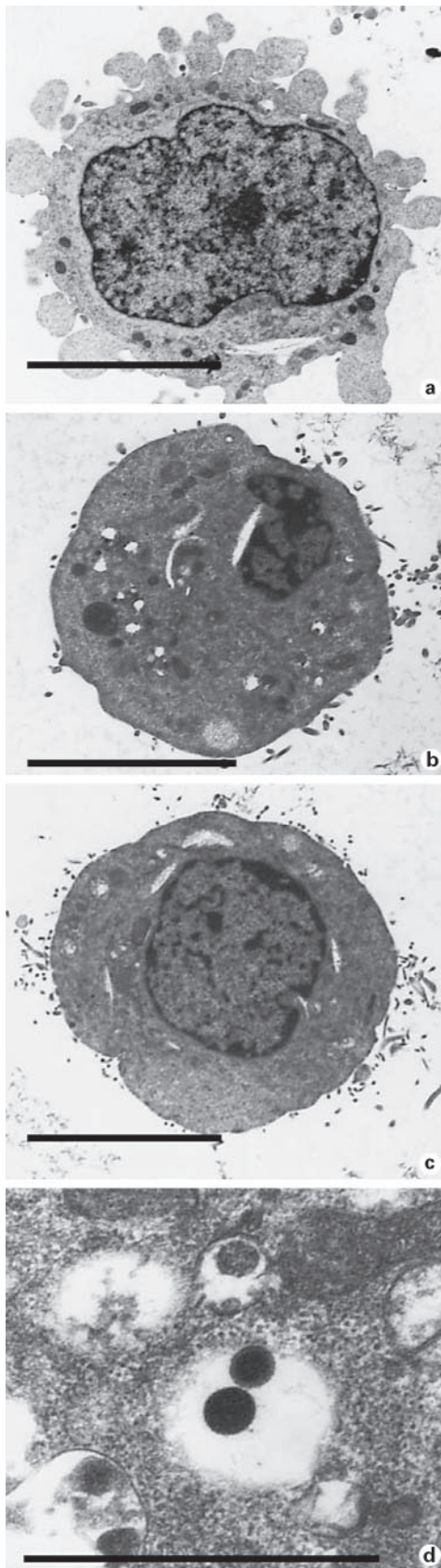


than of salts of these metals. Also, the observed diffraction patterns were not consistent with an organometallic structure. The production of even nanometer-sized metallic particles implies the assembly of a significant number of metal atoms. For example, the volume of a 1-nm diameter Cu particle is approximately equivalent to 10 Cu (or 20  $\alpha$ -Fe) unit cells [Borchardt-Ott, 1993]. Given that FCC and BCC metals contain four and two atoms per unit cell, respectively [Borchardt-Ott, 1993], these data suggest that a particle containing  $\sim 40$  atoms is formed regardless of the lattice type. Furthermore, the very fact that the metallic nanoparticles exist implies that the environment in which they formed prevented both oxidation and coarsening of the particles.

#### *PNCs Cause Death of Cancer Cells*

Cultured cancer cells were sensitive to PNCs. Following incubation with PNCs for 20 h, the viability of R98 and RG2 glioma cells declined by 90% and 75%, respectively, whereas that of rat astrocytes decreased by only

25% (fig. 6a). Cells exposed to PNCs exhibited morphological characteristics consistent with cell death, such as loss of adherence, shrinking/rounding, nuclear condensation and budding from cell bodies (fig. 6c, d). PNC-induced cell damage was comparable to the effect of  $1 \mu\text{M}$  staurosporine, a potent apoptotic reagent [Xue et al., 2003] (fig. 6d). The signs of cell death were confirmed by TEM (fig. 7). Cells undergoing apoptosis displayed green fluorescence (fluorescein isothiocyanate; FITC), whereas dead cells displayed both green and red (propidium iodide) fluorescence (fig. 6e). PNCs also affected the viability of Hs683 (human brain glioma), H9c2[2-1] (rat heart myocardium), 27FR (rat skin fibroblast), and SVGp12 (human brain astroglia) cells (data not shown). The viability of cultured RG2 glioma cells was also affected by PNCs isolated from blood plasma (from a healthy human, dog or rabbit; fig. 6f), and complete suppression of growth required approximately  $1 \times 10^{12}$  PNCs/ml, a concentration that is  $\leq 10\%$  of that found in a healthy animal. PNCs did not significantly alter solution pH.



## Discussion

PNCs consist of 1- to 2-nm metal nanoparticles that contain 40–300 atoms. Given that proteons contain both PNCs and fragments of the Hb  $\alpha$ -chain (fig. 2), we conclude that PNCs play an important role in capturing Hb released to blood plasma. Released Hb is normally captured by haptoglobin, which is then recognized by Hb scavenger receptors and endocytosed by macrophages [Kristiansen et al., 2001]. We speculate that when haptoglobin is depleted during critically elevated hemolysis [Deiss, 1999], released Hb is collected by PNCs. We estimate that approximately  $7 \times 10^{13}$  PNCs/ml are present in human blood, and that only approximately 0.004% of the entire PNC pool is normally linked to proteins to form proteons. On average, a 160-nm diameter proteon can bind approximately 100,000 protein molecules that are the size of Hb. TEM data indicated that blood contains abundant copper nanoparticles, suggesting that proteons result from the nucleation and growth [Eaton and Hofrichter, 1990] of misfolded Hb on copper PNCs. This process may offer insights into the mechanisms of some blood disorders associated with intravascular hemolysis, which results in Hb aggregation [Schluter and Drenckhahn, 1986; Kannan et al., 1988; Papalexis et al., 2001]. Indeed, copper plays a critical role in other protein conformation-based disorders such as prion disease, Parkinson's disease, Alzheimer's disease and familial amyotrophic lateral sclerosis [Brown et al., 1997].

The molecular mechanisms of toxicity observed with cultured mammalian cells exposed to filtrates of blood plasma remain unknown, and little is known about the effects of metal nanoparticles on living cells. We suggest that the strong protein-scavenging properties of metal nanoparticles may reflect their importance in both cell homeostasis and disease [Schmid, 1992; Liu and Xu, 2002].

## Acknowledgements

We thank Barry Erlick, Nancy Cox, Barry Carter, and Arnold Mandell for helpful discussions.

**Fig. 7.** Electron micrographs of RG2 brain glioma cells. A cell before (a) and after (b–d) exposure to  $7.7 \times 10^{11}$  PNCs/ml for 20 min. Scale bars: a–c 5  $\mu$ m; d 1  $\mu$ m.

## References

- Borchardt-Ott, W. (1993) Crystallography. Springer-Verlag, New York.
- Brown, D.R., K. Qin, J.W. Herms, A. Madlung, J. Manson, R. Strome, P.E. Fraser, T. Kruck, A. von Bohlen, W. Schulz-Schaeffer, A. Giese, D. Westaway, H. Kretzschmar (1997) The cellular prion protein binds copper in vivo. *Nature* 390: 684–687.
- Carrel, R.W., D.A. Lomas (1997) Conformational disease. *Lancet* 350: 134–138.
- Deiss, A. (1999) in G.R. Lee, J. Foerster, J. Lukens, F. Paraskevas, J.P. Greer, G.M. Rodgers, M.M. Wintrobe (eds): *Wintrobe's Clinical Hematology*; Williams & Wilkins, Baltimore, pp 267–299.
- Eaton, W.A., J. Hofrichter (1990) Sickle cell hemoglobin polymerization. *Adv Protein Chem* 40: 63–279.
- International Centre for Diffraction Data (2001) Powder Diffraction File, ICDD, Newtown Square.
- H.M.N.H. Irving, R.H. Al-Jarrah (1975) The extraction of various metals as their anionic complexes with EDTA by solutions of aliquat-336 chloride in 1,2-dichloroethane. *Anal Chim Acta* 74: 321–331.
- Jarman, M. (1970) *Examples in quantitative zoology*. Edward Arnold, London.
- Kannan, R., R. Labotka, P.S. Low (1988) Isolation and characterization of the hemichrome stabilized membrane-protein aggregates from sickle erythrocytes – major site of autologous antibody-binding. *J Biol Chem* 263: 13766–13773.
- Kelly, J.W. (1996) Alternative conformations of amyloidogenic proteins govern their behavior. *Curr Opin Struct Biol* 6: 11–17.
- Korth, C., B. Stierli, P. Streit, M. Moser, O. Schaller, R. Fischer, W. Schulz-Schaeffer, H. Kretzschmar, A. Raeber, U. Braun, F. Ehrensperger, S. Hornemann, R. Glockshuber, R. Riek, M. Billeter, K. Wüthrich, B. Oesch (1997). Prion (PrPSc)-specific epitope defined by a monoclonal antibody. *Nature* 390: 74–77.
- Kristiansen, M., J.H. Graversen, C. Jacobsen, O. Sonne, H. Hoffman, S.K. Law, S.K. Moestrup (2001) Identification of the haemoglobin scavenger receptor. *Nature* 409: 198–201.
- Kyte, J., R. Doolittle (1982) A simple method for displaying the hydropathic character of a protein. *J Mol Biol* 157: 105–132.
- Liu, C., H. Xu (2002) The metal site as a template for the metalloprotein structure formation. *J Inorg Biochem* 88: 77–86.
- Logan, T.M., Y. Theriault, S.W. Fesik (1994) Structural characterization of the FK506 binding protein unfolded in urea and guanidine hydrochloride. *J Mol Biol* 236: 637–648.
- Papalexis, V., M. Siomos, N. Campanale, X. Guo, G. Kocak, M. Foley, L. Tilley (2001) Histidine-rich protein 2 of the malaria parasite, *Plasmodium falciparum*, is involved in detoxification of the by-products of haemoglobin degradation. *Mol Biochem Parasitol* 115: 77–86.
- Saborio, G.P., B. Permanne, C. Soto (2001) Sensitive detection of pathological prion protein by cyclic amplification of protein misfolding. *Nature* 411: 810–813.
- Schluter, K., D. Drenckhahn (1986) Co-clustering of denatured hemoglobin with band-3 – its role in binding of autoantibodies against band-3 to abnormal and aged erythrocytes. *Proc Natl Acad Sci USA* 83: 6137–6141.
- Schmid, G. (1992) Large clusters and colloids. Metals in the embryonic state. *Chem Rev* 92: 1709–1727.
- Vonehren, G. (1966) Translational variations in amino acid sequence of alpha-chain of rabbit hemoglobin. *Cold Spring Harb Symp Quant Biol* 31: 705–711.
- Xue, L.-Y., S.-M. Chiu, N.L. Oleinick (2003) Staurosporine-induced death of MCF-7 human breast cancer cells: A distinction between caspase-3-dependent steps of apoptosis and the critical lethal lesions. *Exp Cell Res* 283: 135–145.